NATIONAL AERONAUTICS AND SPACE ADMINISTRATION

Technical Report 32-1448

Shock-Wave Structure of a Gas Having Rotational and Vibrational Relaxation

R. Passamaneck

JET PROPULSION LABORATORY
CALIFORNIA INSTITUTE OF TECHNOLOGY
PASADENA, CALIFORNIA

February 1, 1970

NATIONAL AERONAUTICS AND SPACE ADMINISTRATION

Technical Report 32-1448

Shock-Wave Structure of a Gas Having Rotational and Vibrational Relaxation

R. Passamaneck

JET PROPULSION LABORATORY
CALIFORNIA INSTITUTE OF TECHNOLOGY
PASADENA, CALIFORNIA

February 1, 1970

Prepared Under Contract No. NAS 7-100
National Aeronautics and Space Administration

Foreword

The work described in this report was performed by the Environmental Sciences Division of the Jet Propulsion Laboratory.

Contents

Figures

Abstract

One-dimensional Navier-Stokes equations are used along with two relaxation equations to solve the shock-wave structure for a gas having both rotational and vibrational modes of relaxation. The characteristic relaxation times, as well as Mach number, are varied in order to note the corresponding nonequilibrium effects. Viscosity and heat conduction coefficients are allowed to vary as functions of temperature.

The results presented were obtained by numerical integration of a nonlinear set of three differential equations of a boundary value type in which both boundaries exhibited singularities.

Shock-Wave Structure of a Gas Having Rotational and Vibrational Relaxation

I. Introduction

The structure of a shock wave is solved by assuming that the Navier-Stokes equations and two additional equations for rotational and vibrational relaxation rates apply. The gas properties can be assumed to be either ideal with constant heat capacities and viscosity or real with nonconstant heat capacities and viscosity as an empirical linear function of the appropriate temperature mode. This is an extension of the work performed in Ref. 1, but differs from their extension, Ref. 2, in that no coupling between rotation and vibration occurs. The elimination of this coupling mode seems reasonable, since it could only be realized through a collision between two molecules which, in fact, is a translation process. Therefore, the following treatment will involve only translational–rotational and translational–vibrational coupling. This simplification will be useful in future work which will include additional nonequilibrium processes such as dissociation and ionization. It should be noted, however, that the validity of the solution is questionable if the gradients become too large, since the Navier-Stokes equations are not valid for this regime.

This type of solution to the shock-wave structure is in contrast to the more popular technique, the two-step model, of assuming a discontinuous shock wave in which the translational and rotational temperatures are "shocked" and the vibrational temperature remains at the free stream condition. A relaxation region then occurs in which the vibrational temperature equilibrates with the translational and rotational temperature. A shock-structure solution of the type reported herein would be useful when nonequilibrium effects are known to exist and when the density is low, as in the Mars entry problem.

A number of cases were run which covered an order of magnitude in vibrational relaxation time and a factor of two in rotational relaxation time. The examples shown in this report indicate clearly when the two-step model is sufficient or when the complete shock structure must be solved for a solution. An additional advantage of this type of solution, aside from accuracy, is that the modified Rankine-Hugonoit conditions across the shock wave, needed for a solution to a shock-layer problem when the shock-wave thickness can not be assumed to be small,

are provided. This effect can be seen by imagining that the downstream shock conditions for an oblique shock wave "slip" along the shock due to the presence of the tangential velocity.

II. Equations of Motion

The conservation equations of continuity, linear momentum, and energy, including viscosity and heat conduction terms, for a one-dimensional steady flow in the x direction are

$$\frac{d(\rho u)}{dx} = 0 \tag{1}$$

$$\rho u \frac{du}{dx} + \frac{dp}{dx} - \frac{d}{dx}\left(\frac{4}{3}\mu \frac{du}{dx}\right) = 0 \tag{2}$$

$$\rho u\, c_p \frac{dT}{dx} - u\frac{dp}{dx} - \frac{d}{dx}\left(\lambda \frac{dT}{dx}\right) - \frac{4}{3}\mu\left(\frac{du}{dx}\right)^2 = 0 \tag{3}$$

The continuity equation can be easily integrated, as

$$\rho u = m \tag{4}$$

where m is the constant of integration and is equal to the mass flux per unit area.

Using the result of Eq. (4), the linear momentum equation can be integrated at once.

$$\rho u^2 + p - \frac{4}{3}\mu \frac{du}{dx} = P \tag{5}$$

where P is the constant of integration and must be equal to $p_1 + \rho_1 u_1^2$ or $p_2 + \rho_2 u_2$ since far upstream or far downstream the gardients must vanish and the equation regains its Rankine-Hugonoit relationship.

The integration of the energy equation cannot be performed directly because of the nonlinearity of the first derivative. It can be made integrable, however, if one multiplies the linear momentum equation by u and adds it to the energy equation; i.e.,

$$\rho u\left\{c_p \frac{dT}{dx} + u\frac{du}{dx}\right\} - \frac{d}{dx}\left(\lambda \frac{dT}{dx}\right) - \frac{4}{3}\mu\left\{\left(\frac{du}{dx}\right)^2 + u\frac{d}{dx}\left(\frac{du}{dx}\right)\right\} = 0 \tag{6}$$

The partitioning of the internal energy of the gas into the various modes will be accomplished in Eq. (6). The temperature gradient will, therefore, be split into its translational, rotational and vibrational parts; i.e.,

$$c_p \frac{dT}{dx} = c_{p_T}\frac{dT_T}{dx} + c_{p_R}\frac{dT_R}{dx} + c_{p_V}\frac{dT_V}{dx} \tag{7}$$

and

$$\lambda \frac{dT}{dx} = \lambda_T \frac{dT_T}{dx} + \lambda_R \frac{dT_R}{dx} + \lambda_V \frac{dT_V}{dx} \tag{8}$$

Substituting these into Eq. (6) and then integrating, yield

$$\rho u^3 + 2\rho u\{c_{p_T} T_T + c_{p_R} T_R + c_{p_V} T_V\} - 2\left\{\lambda_T \frac{dT_T}{dx} + \lambda_R \frac{dT_R}{dx} + \lambda_V \frac{dT_V}{dx}\right\} - 2\left(\frac{4}{3}\mu\right) u \frac{du}{dx} = Q \tag{9}$$

where Q is a constant of integration and must be equal to the total enthalpy divided by the mass flux per unit area. The energy equation, as did the linear momentum equation, has the Rankine-Hugonoit relationship in the limit of far upstream and far downstream from the shock wave.

As can be seen, the number of unknown variables is five, whereas there are only three equations. In order to obtain two additional equations, it will be assumed that the Landau-Teller relaxation model for the rotational and vibrational temperatures is valid.

$$\frac{DT_R}{Dt} = \frac{T_T - T_R}{\omega_R}$$

for rotation and

$$\frac{DT_V}{Dt} = \frac{T_T - T_V}{\omega_V}$$

for vibration, where D/Dt is the material derivative. It should be noted that the "bath temperature" is that of translation and there is no rotation-vibration coupling except indirectly through the translation temperature. The characteristic relaxation times for rotation and vibration are represented by ω_R and ω_V, respectively. The relaxation times can be related to the mean free path L, the

mean molecular speed c and the number of collisions N_i required for the characteristic relaxation time by

$$\omega_i = \frac{N_i L}{c}$$

The values for ω_i can be related to viscosity and pressure by introducing the following equations:

$$\mu = \beta_\mu \rho c L, p = \rho R T_T \qquad \text{and} \qquad c = \left(\frac{8 R T_T}{\pi}\right)^{1/2}$$

where β_μ will be taken as equal to ½. Substitution yields

$$\omega_i = \frac{\pi}{4} \frac{N_i \mu}{p} \tag{10}$$

Substituting this equation in the relaxation equations, and noting that $D/Dt = u\, d/dx$ for one-dimensional flow, we have

$$u \frac{dT_R}{dx} = \frac{T_T - T_R}{\frac{\pi N_R}{4} \frac{\mu}{p}} \tag{11}$$

for rotation, and

$$u \frac{dT_V}{dx} = \frac{T_T - T_V}{\frac{\pi N_V}{4} \frac{\mu}{p}} \tag{12}$$

for vibration. Typical values for the number of collisions required for equilibration would be of O(10) for rotation and of O(1000) for vibration. The values of N_V vary greatly depending on the type of molecules involved. In addition, N_V has a strong pressure dependence and a weak temperature dependence. The values for N_V are obtained experimentally as no valid theoretical approach has yet been devised. A complete discussion of vibrational relaxation is presented in Ref. 2. Similar results would probably be obtained for rotational relaxation times; but, experimental values do not exist, except over a limited low temperature range.

The complete set of equations now consist of Eqs. (4, 5, 9, 11, and 12) and an equation of state. The equation of state has been assumed to be that of an ideal gas, $p = \rho R T_T$. The equations will be reduced to a non-dimensional form for computational purposes. The non-dimensional quantities are introduced as follows:

$$v = \frac{mu}{P}, \qquad r = \frac{P\rho}{m^2}, \qquad \tau = \frac{m^2 R T_T}{P^2}, \qquad \phi = \frac{m^2 R T_R}{P^2}$$

$$\theta = \frac{m^2 R T_V}{P^2}, \qquad \sigma = \frac{p}{P}, \qquad \alpha = \frac{mQ}{P^2}, \qquad c_T = \frac{c_{v_T}}{R},$$

$$c_R = \frac{c_{vR}}{R} \qquad \text{and} \qquad c_V = \frac{c_{v_V}}{R},$$

Also form the following transport lengths and the non-dimensional counterparts:

$$L_\mu = \frac{\mu}{m}, \qquad L_T = \frac{\lambda_T}{mR}, \qquad L_R = \frac{\lambda_R}{mR}, \qquad L_V = \frac{\lambda_V}{mR}$$

and

$$\gamma_T = \frac{L_T}{L_\mu}, \qquad \gamma_R = \frac{L_R}{L_\mu}, \qquad \gamma_V = \frac{L_V}{L_\mu} \qquad \text{and} \qquad y = \frac{\tau^* x}{L_\mu^*}$$

where L_μ^* is a reference transport length evaluated at a reference temperature τ^*.

The equations now become

$$rv = 1 \tag{13}$$

$$rv^2 + \sigma - \frac{4}{3}\left(L_\mu \frac{\tau^*}{L_\mu^*}\right)\frac{dv}{dy} = 1$$

$$rv^3 + 2rv\,(c_T\tau + c_R\phi + c_V\theta) + 2\sigma v$$

$$- 2\left[\left(\frac{L_T\tau^*}{L_\mu^*}\right)\frac{d\tau}{dy} + \left(\frac{L_R\tau^*}{L_\mu^*}\right)\frac{d\phi}{dy} + \left(\frac{L_V\tau^*}{L_\mu^*}\right)\frac{d\theta}{dy}\right]$$

$$- \frac{8}{3}\left(\frac{L_\mu\tau^*}{L_\mu^*}\right)v\frac{dv}{dy} = \alpha$$

$$\frac{\tau^*}{L_\mu^*}v^2\frac{d\phi}{dy} = \frac{\tau}{L_\mu}\frac{\tau - \phi}{\frac{\pi N_R}{4}}$$

$$\frac{\tau^*}{L_\mu^*}v^2\frac{d\theta}{dy} = \frac{\tau}{L_\mu}\frac{\tau - \theta}{\frac{\pi N_V}{4}}$$

$$\sigma = r\tau$$

When the viscosity is assumed to be linear[1] and in the form $\mu = (\mu^*/\tau^*)\,\tau$, where μ^* is the viscosity at the reference temperature τ^*, the equations are:

$$rv = 1 \tag{13}$$

$$\frac{4}{3}\tau\frac{dv}{dy} = rv^2 + \sigma - 1 \tag{14}$$

$$2\gamma_T\tau\frac{d\tau}{dy} + 2\gamma_R\tau\frac{d\phi}{dy} + 2\gamma_V\tau\frac{d\theta}{dy} =$$

$$- \frac{8}{3}\tau v\frac{dv}{dy} + rv^3 + 2rv\,(c_T\tau + c_R\phi + c_V\theta)$$

$$+ 2\sigma v - \alpha \tag{15}$$

$$v^2\frac{d\phi}{dy} = \frac{\tau - \phi}{\frac{\pi N_R}{4}} \tag{16}$$

$$v^2\frac{d\theta}{dy} = \frac{\tau - \theta}{\frac{\pi N_V}{4}} \tag{17}$$

$$\sigma = r\tau \tag{18}$$

This set of six equations, of which four are differential and two are algebraic, can be reduced to four differential equations through the elimination of σ and r by use of Eqs. (13) and (18). Carrying this through, one obtains:

$$\frac{4}{3}\tau v\frac{dv}{dy} = v^2 + \tau - v \tag{19}$$

$$2\gamma_T\tau\frac{d\tau}{dy} + 2\gamma_R\tau\frac{d\phi}{dy} + 2\gamma_V\tau\frac{d\theta}{dy} =$$

$$- v^2 + 2v + 2c_T\tau + 2c_R\phi + 2c_V\theta - \alpha \tag{20}$$

Where Eq. (19) has been used to obtain Eq. (20), Eqs. (16) and (17) remain the same since they did not contain σ or τ.

The system of differential equations to be solved are improper since the independent variable y does not appear anywhere in the equations. It is necessary, therefore, to make a change of variable. The convient and logical choice is to let v be the independent variable through the use of Eq. (19). This will reduce the set of four equations in which τ, ϕ, θ, and v are functions of y to a set of three equations in which τ, ϕ, and θ are functions of v. Carrying the transformation through yields

$$\frac{d\phi}{dv} = \frac{16}{3\pi N_R}\frac{\tau\,(\tau - \phi)}{v\,(v^2 + \tau - v)} \tag{21}$$

$$\frac{d\theta}{dv} = \frac{16}{3\pi N_V}\frac{\tau\,(\tau - \theta)}{v\,(v^2 + \tau - v)} \tag{22}$$

and

$$\frac{d\tau}{dv} = \frac{2}{3\gamma_\tau}\frac{v^2\,(-v^2 + 2v + 2c_T\tau + 2c_R\phi + 2c_V\phi - \alpha) - (8\gamma_V/\pi N_V)\,\tau\,(\tau - \theta) - (8\gamma_R/\pi N_R)\,\tau\,(\tau - \phi)}{v\,(v^2 + \tau - v)}$$

This set of differential equations constitutes a two-point boundary value problem with singularities existing at both boundaries.

[1]The linear assumption need not be made; however, the formulation would be more difficult.

III. Solution of Equations

The solution of Eqs. (21–23) by numerical means presents difficulties since both the numerator and denominator are equal to zero at the initial and final boundary. The application of L'Hospital's rule gives the necessary values for

$$\left.\frac{d\theta}{dv}\right|_1 \qquad \text{and} \qquad \left.\frac{d\phi}{dv}\right|_1$$

at the initial boundary.

$$\left.\frac{d\phi}{dv}\right|_1 = \frac{\tau_1 \left.\dfrac{d\tau}{dv}\right|_1}{\dfrac{3\pi N_R}{16} v_1 \left(2v_1 + \left.\dfrac{d\tau}{dv}\right|_1 - 1 \right) + \tau_1}$$

and

$$\left.\frac{d\theta}{dv}\right|_1 = \frac{\tau_1 \left.\dfrac{d\tau}{dv}\right|_1}{\dfrac{3\pi N_V}{16} v_1 \left(2v_1 + \left.\dfrac{d\tau}{dv}\right|_1 - 1 \right) + \tau_1}$$

where the subscript 1 refers to the initial condition. Examination of these equations shows that a value of $d\phi/dv|_1$ and $d\theta/dv|_1$ can only be found if $d\tau/dv|_1$ is known. The application of L'Hospital's rule to $d\tau/dv$ yields a lengthy 4th degree polynomial in $d\tau/dv|_1$. The four solutions to the polynomial are real, but only one is valid; the other three have been extraneously introduced. In all the cases tried, the four solutions followed the same pattern represented in Fig. 1. Consideration of the physics of the problem shows that the value of $d\tau/dv|_1$ has to lay below the singularity line and above the dotted straight line joining the initial and final value of τ. Only one value of $d\tau/dv|_1$ is between these limits. The sensitivity of the singularity makes it necessary to iterate the initial value of $d\tau/dv|_1$ beyond the accuracy of the value given by the polynomial solution.

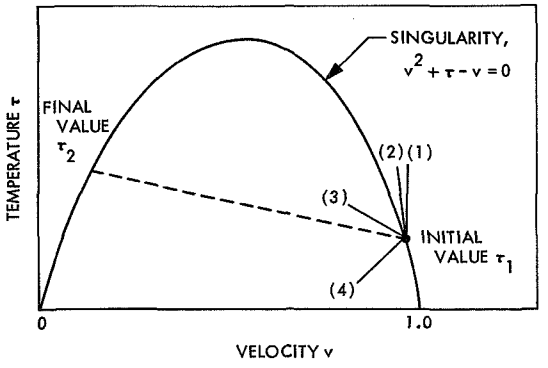

Fig. 1. Initial and final singularities in temperature–velocity space

The value of $d\tau/dv|_1$ was iterated to 16 significant figures, however, the error in τ at the final boundary was about $\pm 10\%$. To improve the solution, it was decided to take the best two solutions: one falling above τ_2 and one falling below τ_2, and examine their differences as one proceeds away from τ_1. The $\Delta\tau$ was examined at each integration step in order to find the integration step where $\Delta\tau < \epsilon$; the next step, however, would make $\Delta\tau > \epsilon$. In all cases, $\epsilon = 10^{-6}$ so that $\Delta\tau$ was slightly less than 10^{-6}. At this point, τ was iterated between the two limits of τ obtained from the previous "best upper" and "best lower" solutions. This iteration would then yield a new best upper and a new best lower solution. This procedure was repeated at every point in which τ was about to exceed 10^{-6} until the second boundary was reached.

Having the solutions of τ, ϕ, and θ as a function of v through Eqs. (21–23), makes it possible to solve for σ and r as a function of v through the use of Eqs. (13) and (18). The solutions of τ, ϕ, θ, σ, r, and v may now be determined as a function of y through an integration of Eq. (19), which was originally used to make the change of independent variable from y to v. Since the $y = 0$ point is arbitrary, it was taken to be at $v = (v_1 + v_2)/2$. A discussion of the results of the various cases will be given in Section IV.

IV. Results

The cases presented are at Mach numbers 1.5, 3.0, and 10.0 with the number of collisions required for rotational equilibration equal to 10 and the number of collisions required for vibrational equilibration equal to 100 and 500. Two additional cases are presented. The first case has a Mach number of 10.0 with the number of collisions required for rotational and vibrational equilibration equal to 5 and 500, respectively. The second case has a Mach number of 3.0 with the number of collisions required for rotational and vibrational equilibrium equal to 10 and 1000, respectively. In all cases, the free-stream conditions correspond to those at an altitude of 150,000 ft with $c_T = 3/2$, $c_R = 1$, $c_V = 1$, $\gamma_T = 15/4$, $\gamma_R = 1$, and $\gamma_V = 1$, and held constant throughout the shock wave.

The three cases with a Mach number of 3.0, $N_R = 10$, and $N_V = 100$, 500, and 1000 shows the effect of vibrational relaxation time on the shock structure. This is shown in Figs. 2, 3, and 4 where the translational, rotational, and vibrational temperature variation is plotted in phase space for $N_V = 100$, 500, and 1000, respectively.

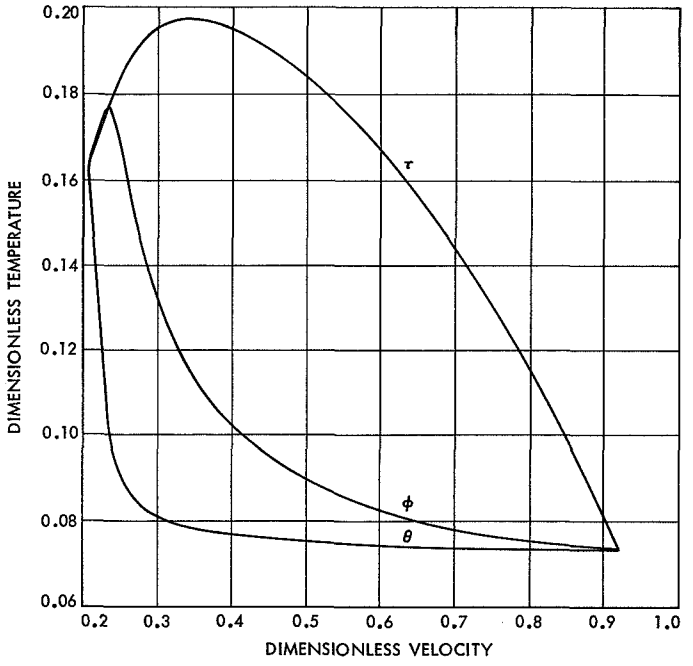

Fig. 2. Temperature vs velocity curves for $M = 3$, $N_R = 10$, and $N_V = 100$

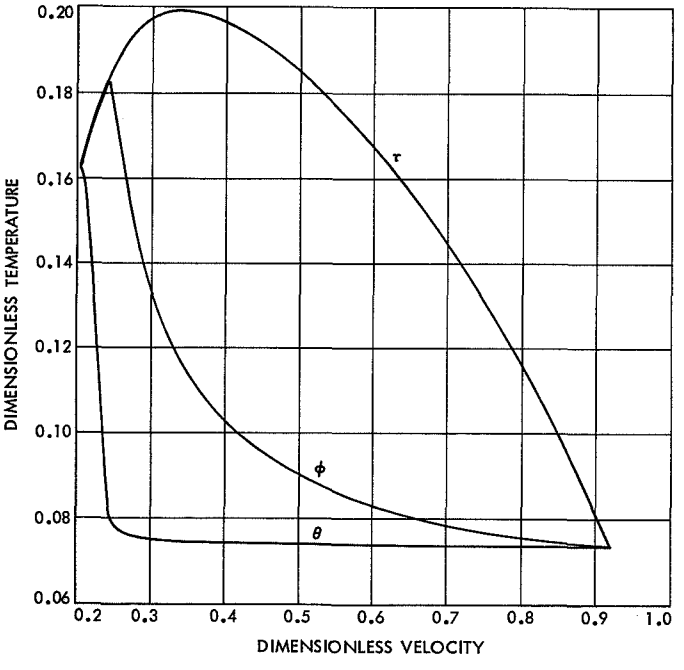

Fig. 3. Temperature vs velocity curves for $M = 3$, $N_R = 10$, and $N_V = 500$

It can be seen that the vibrational temperature rise is delayed longer and longer as the number of collisions for vibrational equilibration is increased. This effect is more noticeable when comparing the $N_V = 100$ and the $N_V = 500$ cases as opposed to comparing the $N_V = 500$ and the $N_V = 1000$ cases, since the first comparison has a multiplication of 5 in N_V and the second comparison has a multiplication of only 2 in N_V. It should also be noted that as N_V is increased, the peaks of translational and rotational temperature are increased and also delayed as is the vibrational temperature rise. Converting from the phase space to the physical space by means of Eq. (19) results in Figs. 5, 6, and 7. Comparing the corresponding figures in phase space and physical space shows the extent to which the "relaxation" part of the shock wave is expanded in the physical space.

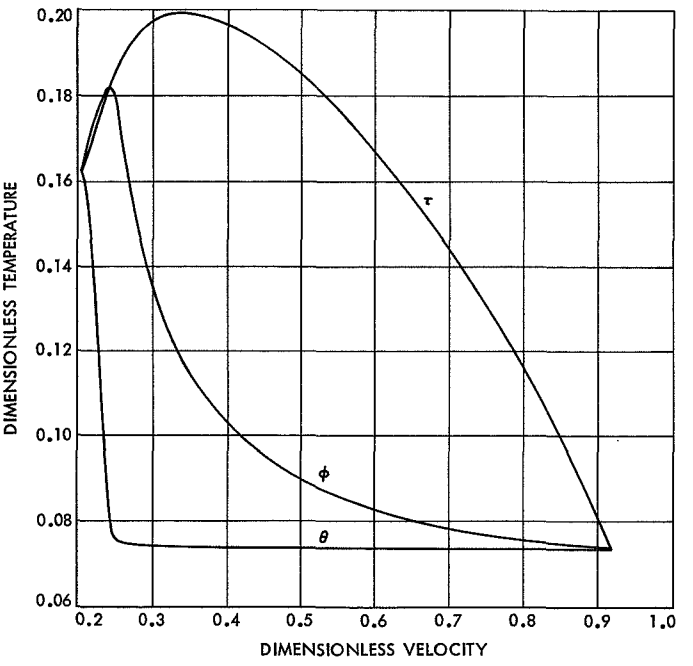

Fig. 4. Temperature vs velocity curves for $M = 3$, $N_R = 10$, and $N_V = 1000$

The density and pressure for $M = 3.0$, $N_R = 10$, and $N_V = 100$ in phase space are shown in Fig. 8; Fig. 9 shows these parameters when they have been converted to physical space. The densities and pressures in phase space and physical space, respectively, for $M = 3.0$, $N_R = 10$, and $N_R = 1000$ are shown in Figs. 10 and 11. In these figures, the effect of converting from the phase space to physical space is quite obvious. Again, as in the temperatures profiles, the relaxation zone has appeared in the physical space. One additional feature for density should be noted in Fig. 11. The inflection in the density curve for $N_V = 1000$ occurs as the vibrational mode starts its change towards equilibrium. This effect is not noticed in the density curve for $N_V = 100$, Fig. 9, since its relax-

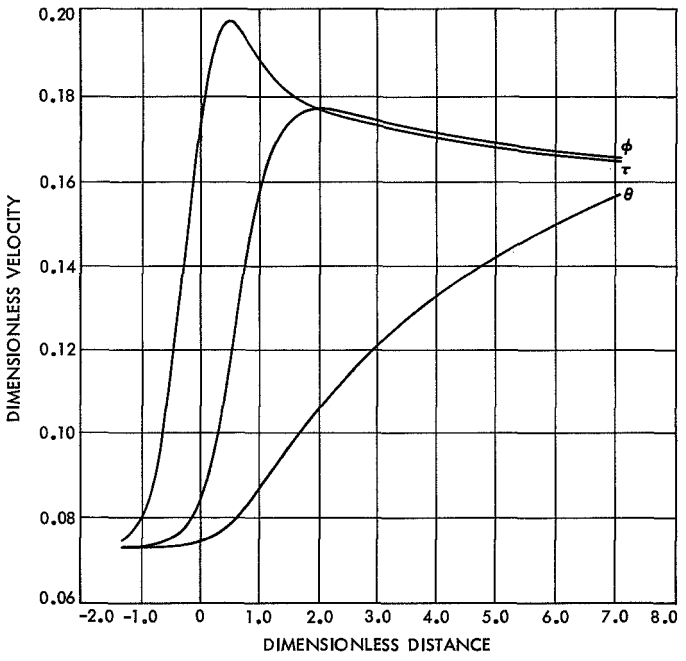

Fig. 5. Temperature vs distance curves for $M = 3$, $N_R = 10$, and $N_V = 100$

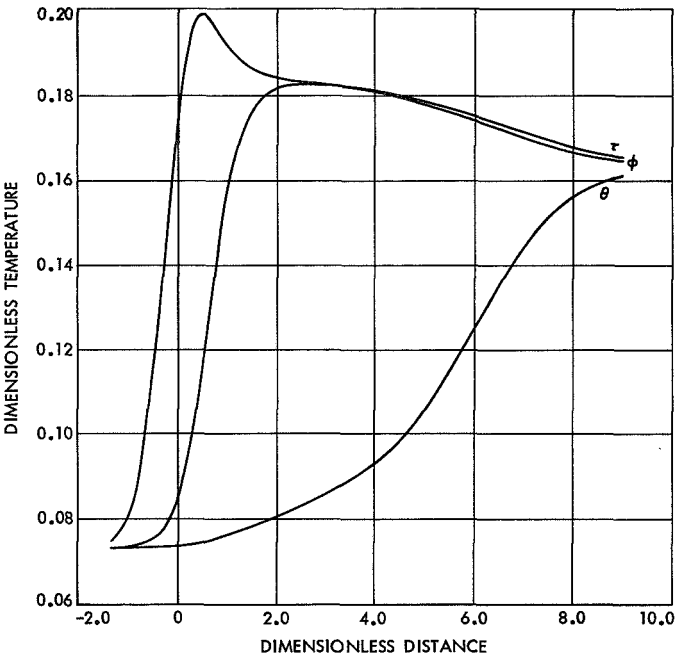

Fig. 6. Temperature vs distance curves for $M = 3$, $N_R = 10$, and $N_V = 500$

ation starts in the steep part of the profile and is, therefore, not significant.

The effect of Mach number on shock structure can be shown in two comparisons. The first comparison is for $N_R = 10$ and $N_V = 100$ with Mach numbers of 1.5, 3.0, and 10.0. Temperature profiles in phase space are shown in Figs. 12, 2, and 13, respectively. It is interesting to note that the effect of increasing only the Mach number is similar to that of increasing only the relaxation time for vibrational equilibration. These same temperature profiles, when they are presented in physical space, are shown in Figs. 14, 5, and 15. The increased overshoot of translational temperature, as the Mach number is increased, is the interesting feature; this is due to the increased amount of kinetic energy that must be absorbed in the early part of the shock by the translational temperature. The density and pressure profiles in phase space are shown in Figs. 16, 8, and 17; Figs. 18, 9, and 19 show these profiles in physical space. These curves show no secondary relaxation region as did the case for $N_V = 1000$, with $M = 3.0$, and $N_R = 10$ as shown in Fig. 11 (special note should be taken of the density profile). The second comparison is for the same value of N_R and the same Mach number values with N_V now equal to 500. The temperature profiles in phase space for these cases are shown in Figs. 20, 3, and 21. The same effect, as was pointed out for the cases with $N_V = 100$, is also present, although not

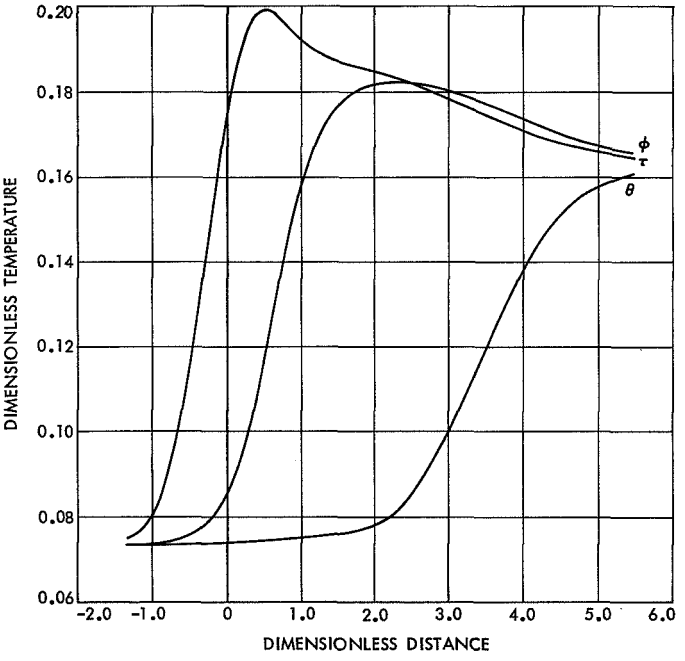

Fig. 7. Temperature vs distance curves for $M = 3$, $N_R = 10$, and $N_V = 1000$

to such a great extent. The temperature profiles in physical space are shown in Figs. 22, 6, and 23. Density and pressure profiles are shown in phase space in Figs. 24 and 25 (the profiles for the $M = 3.0$ case have been

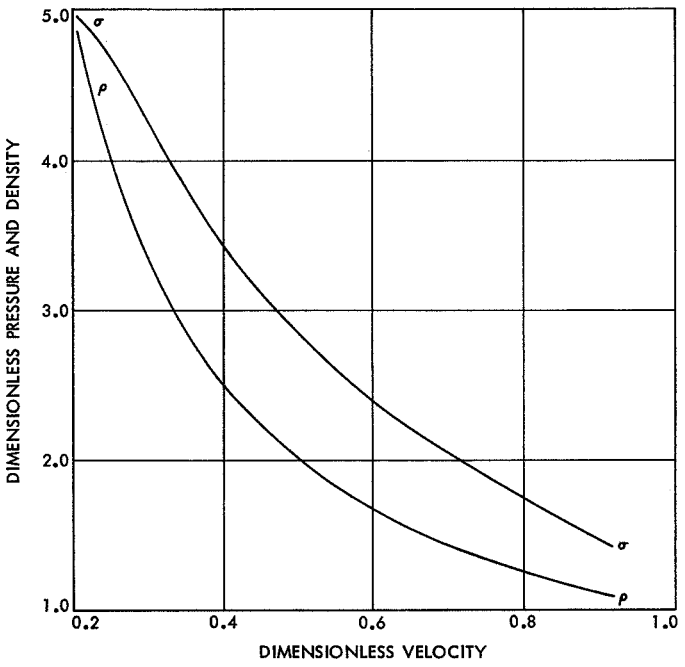

Fig. 8. Pressure and density vs velocity curves for $M = 3$, $N_R = 10$, and $N_V = 100$

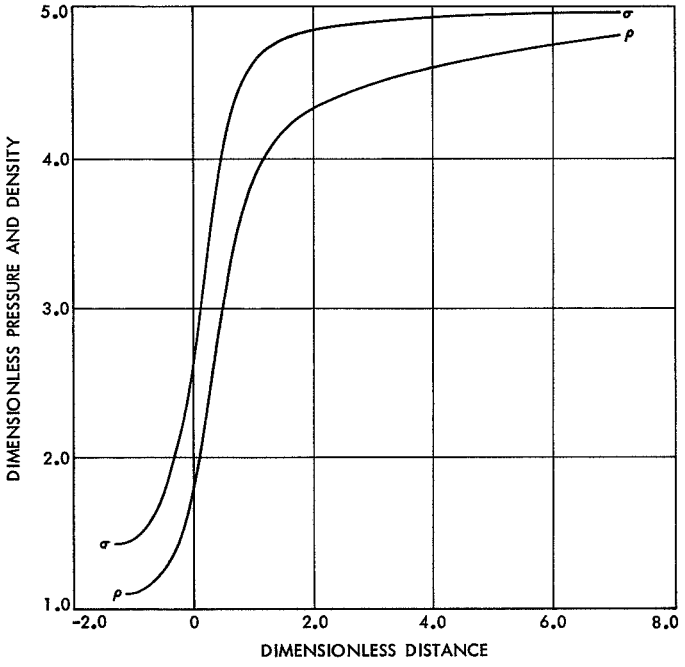

Fig. 9. Pressure and density vs distance curves for $M = 3$, $N_R = 10$, and $N_V = 100$

omitted) and in physical space in Figs. 26 and 27. In contrast to the cases in the first comparison, a relaxation region has appeared and can be seen in both the density and pressure profiles in physical space.

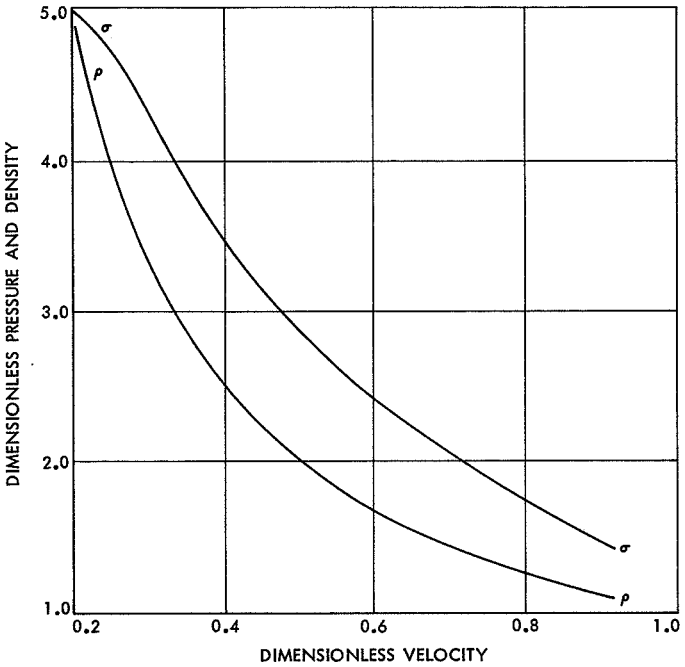

Fig. 10. Pressure and density vs velocity curves for $M = 3$, $N_R = 10$, and $N_V = 1000$

One additional case in which $N_R = 5$, $N_V = 500$, and a Mach number of 10.0 is presented in Figs. 28 and 29 for temperature profiles in phase space and physical space, respectively. Comparing these illustrations with Figs. 21 and 23 for $N_V = 500$ and Mach number of 10.0 but with $N_R = 10$ shows a marked difference in the shock wave thickness. This is shown in the physical space where for $N_R = 5$ the rotational temperature equilibrates with translational temperature at $y \cong 0.82$; whereas for $N_R = 10$, the equilibration does not take place until $y \cong 1.30$. The equilibration for vibrational temperature is correspondingly longer for $N_R = 10$ as compared to $N_R = 5$.

V. Conclusions

The cases presented show that for all relaxation times in the vibrational mode, there was a significant rise in the vibrational temperature before the rotational temperature equilibrated with the translational temperature. As can be seen in Figs. 5, 6, and 7 for $N_R = 100$, 500, and 1000 the percentage rise in vibrational temperature before rotation-translation equilibration was 45, 16.5, and 13.5%, respectively. For this reason, a shock-structure analysis is preferred to the "two-step" model when accuracy is required to better than say 10%. This last statement, of course, only holds for $N_V \geqq 500$. For $N_V < 500$, the two-

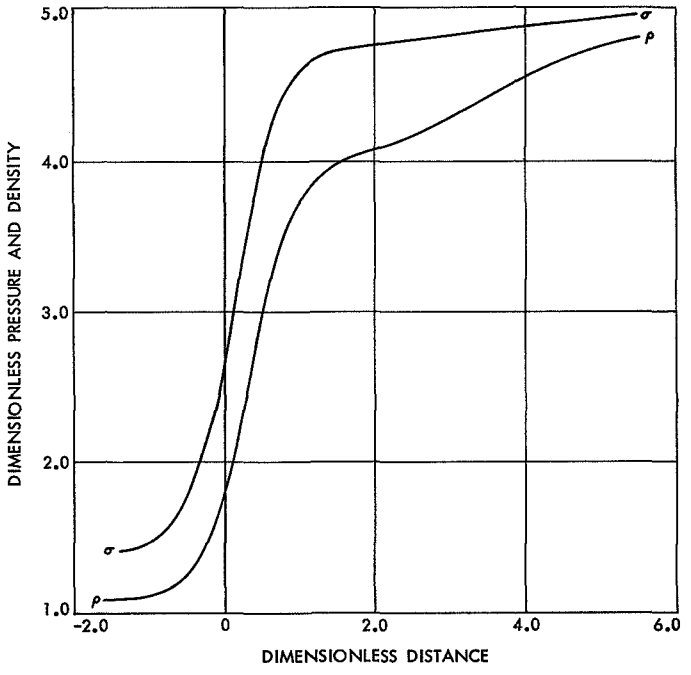

Fig. 11. Pressure and density vs distance curves for $M = 3$, $N_R = 10$, and $N_V = 1000$

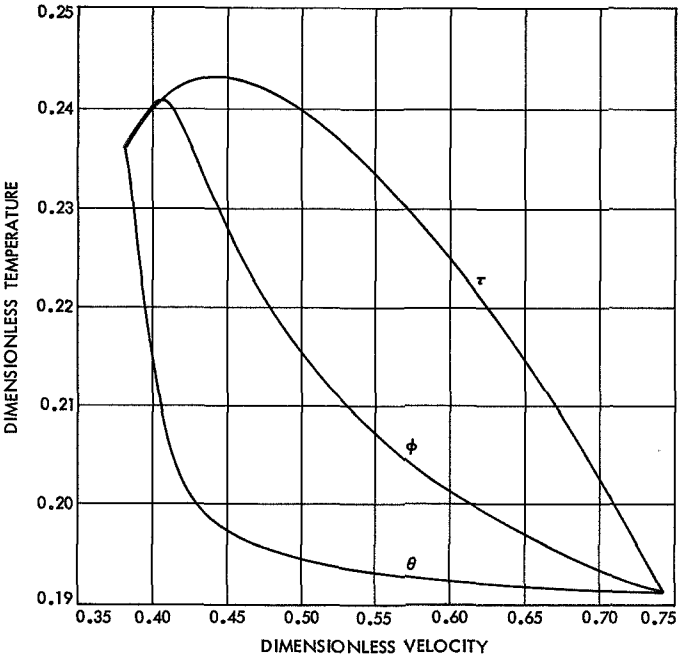

Fig. 12. Temperature vs velocity curves for $M = 1.5$, $N_R = 10$, and $N_V = 100$

step model is completely unsatisfactory and the only recourse is a shock-structure analysis.

The values of N_R were not varied much since they are generally accepted to be in the neighborhood of from 5 to 10 collisions. For a given value of N_V, the two-step model will be better as N_R is decreased and will, conversely, be worse as N_R is increased. In this respect, N_R plays a large role as to whether or not the two-step model is applicable to a given problem.

As stated earlier, care should be taken when using the shock-structure analysis for high Mach numbers and high densities, since large gradients could introduce errors into the results through the Navier-Stokes equations. Whether significant errors occur is a function of the values for N_R and N_V as well as the Mach number; therefore, each case must be examined individually.

It is clear that this problem could be extended to include dissociation, and possibly ionization, by the use of an augmented equation of state along with a rate equation for dissociation, or ionization. For example, Lighthill's ideal dissociating gas could be used for the equation of state in the dissociation region and a similar equation could be applied in the region in which ionization occurs.

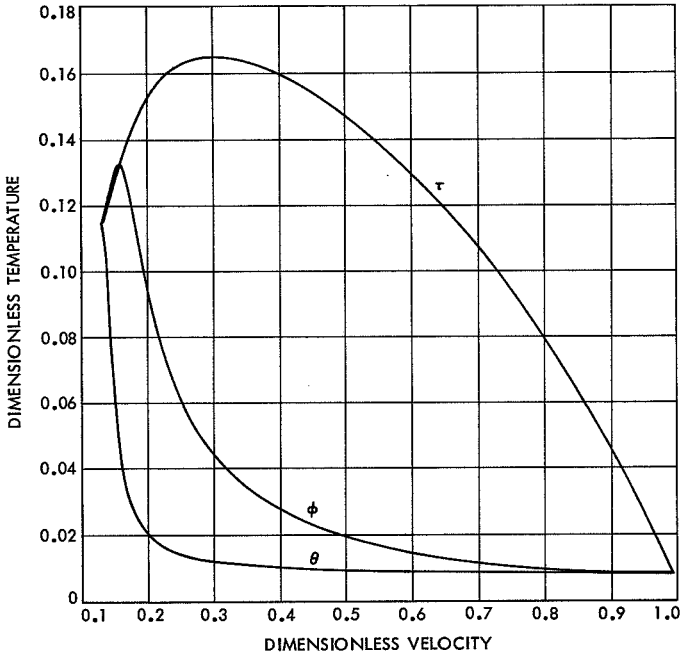

Fig. 13. Temperature vs velocity curves for $M = 10$, $N_R = 10$, and $N_V = 100$

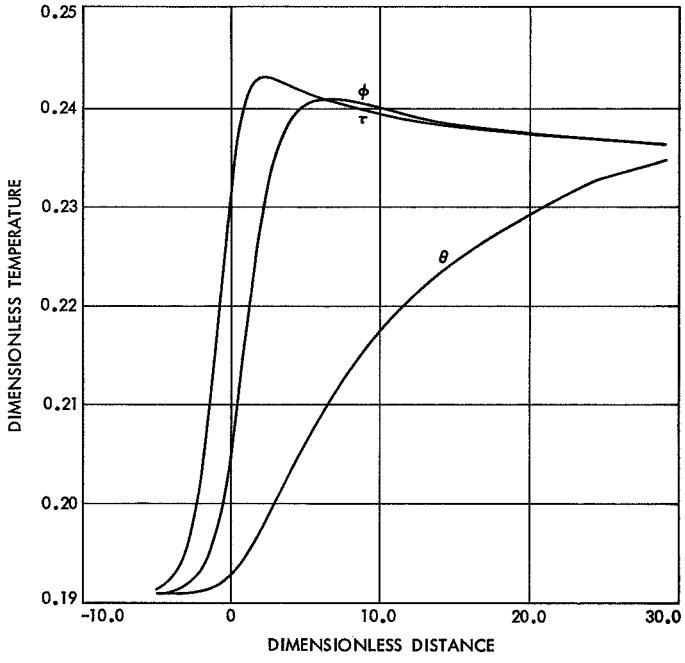

Fig. 14. Temperature vs distance curves for $M = 1.5$, $N_R = 10$, and $N_V = 100$

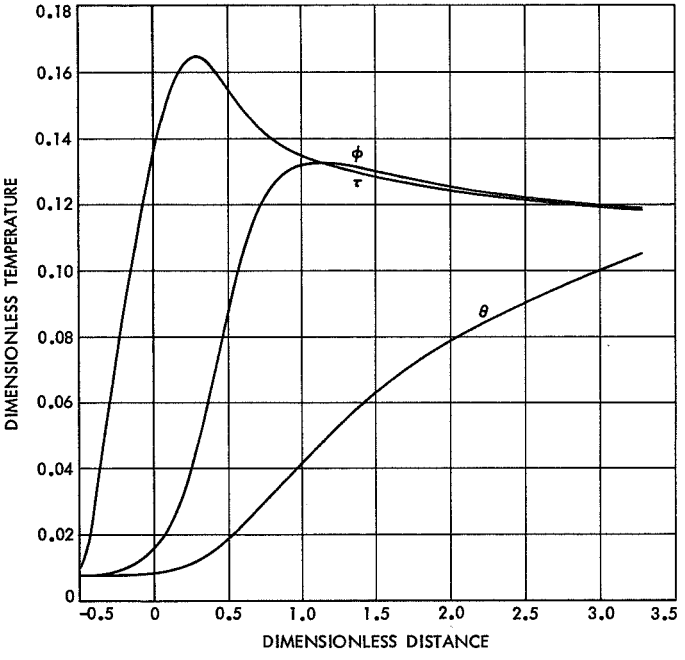

Fig. 15. Temperature vs distance curves for $M = 10$, $N_R = 10$, and $N_V = 100$

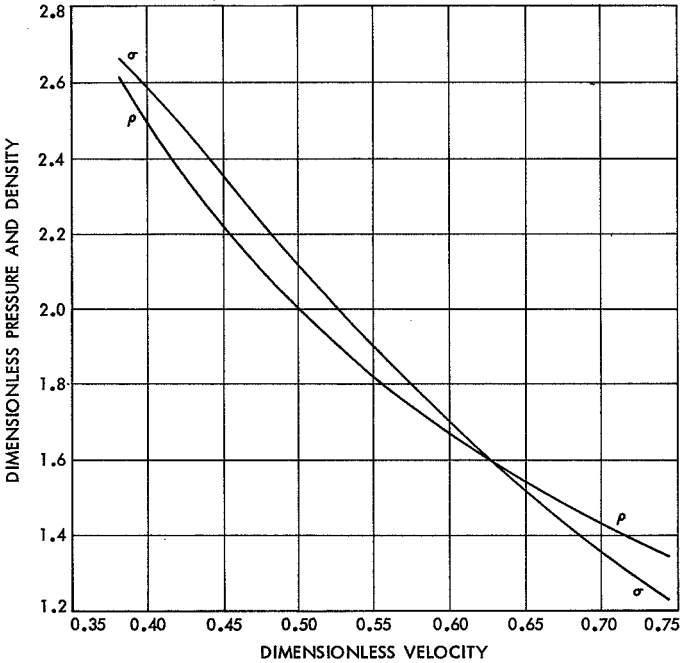

Fig. 16. Pressure and density vs velocity curves for $M = 1.5$, $N_R = 10$, and $N_V = 100$

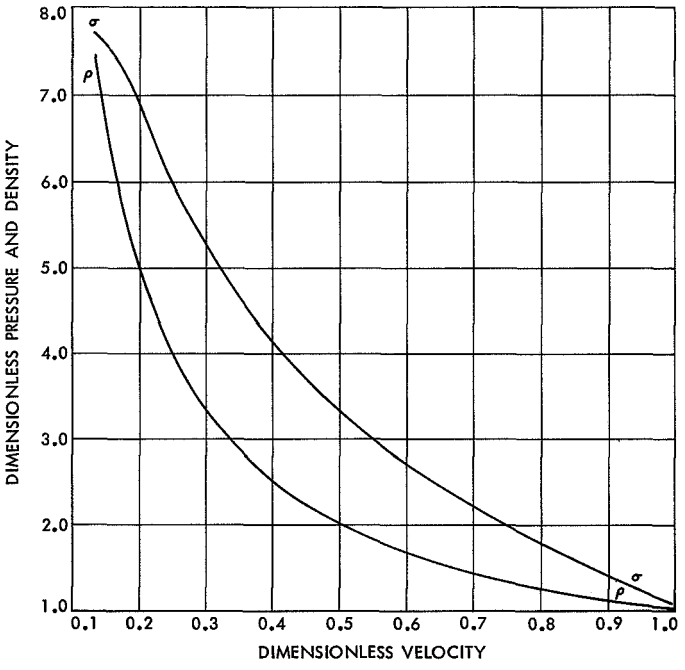

Fig. 17. Pressure and density vs velocity curves for $M = 10$, $N_R = 10$, and $N_V = 100$

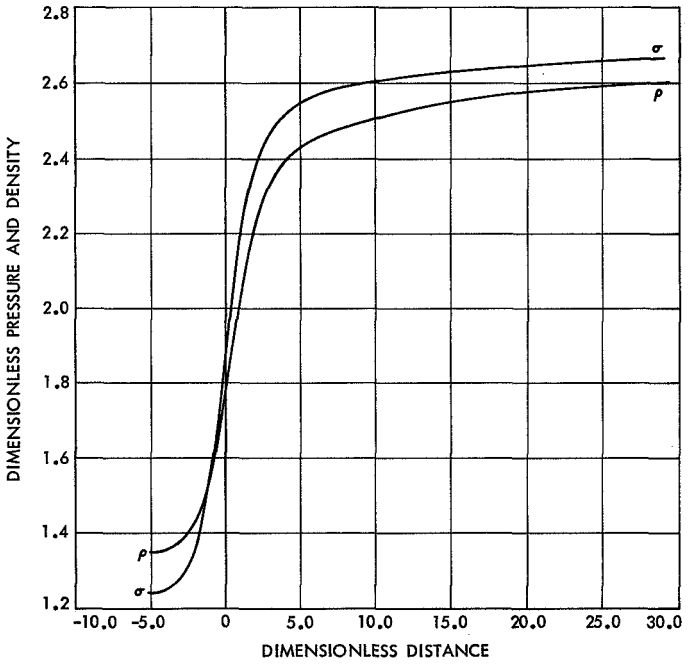

Fig. 18. Pressure and density vs distance curves for $M = 1.5$, $N_R = 10$, and $N_V = 100$

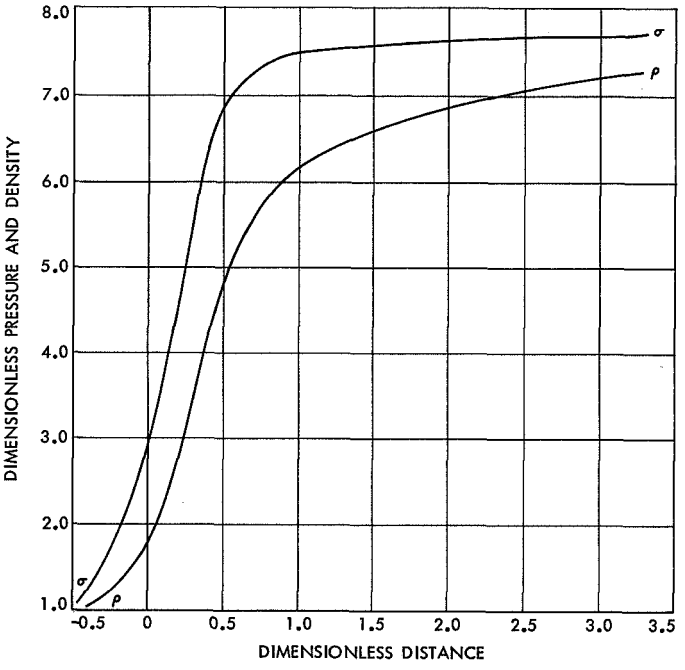

Fig. 19. Pressure and density vs distance curves for $M = 10$, $N_R = 10$, and $N_V = 100$

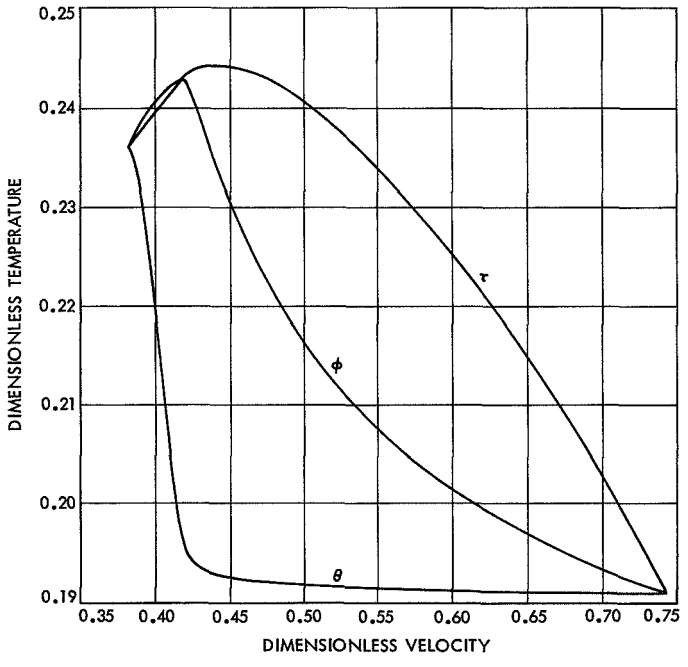

Fig. 20. Temperature vs velocity curves for $M = 1.5$, $N_R = 10$, and $N_V = 500$

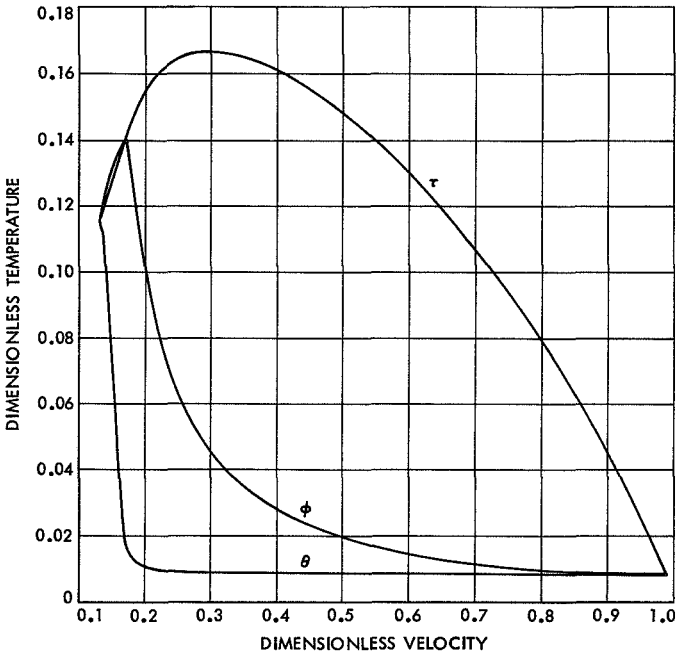

Fig. 21. Temperature vs velocity curves for $M = 10$, $N_R = 10$, and $N_V = 500$

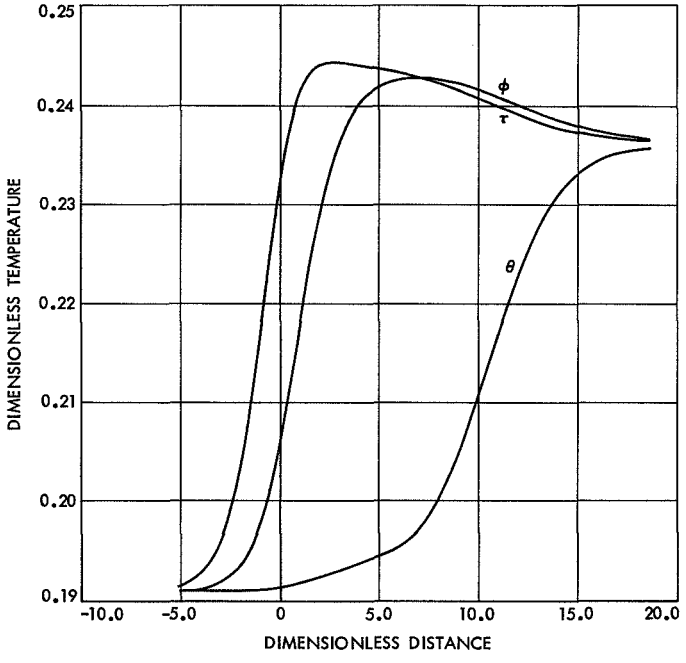

Fig. 22. Temperature vs distance curves for $M = 1.5$, $N_R = 10$, and $N_V = 500$

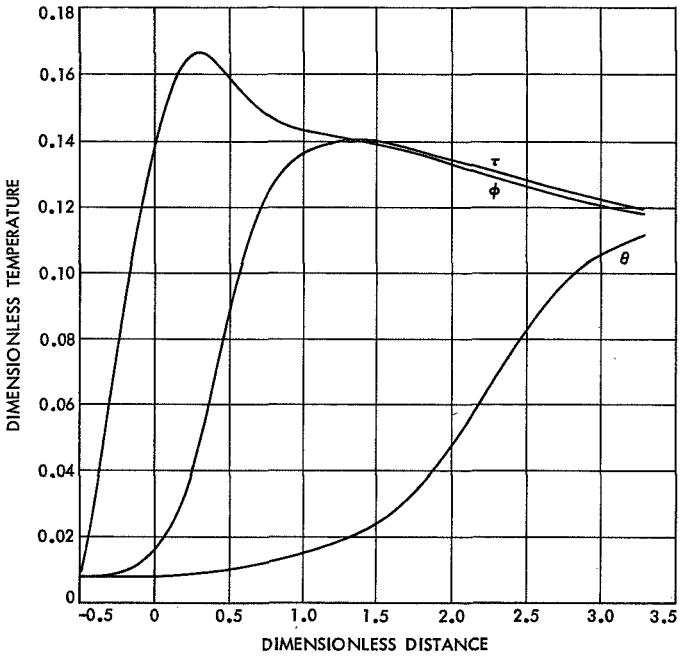

Fig. 23. Temperature vs distance curves for $M = 10$, $N_R = 10$, and $N_V = 500$

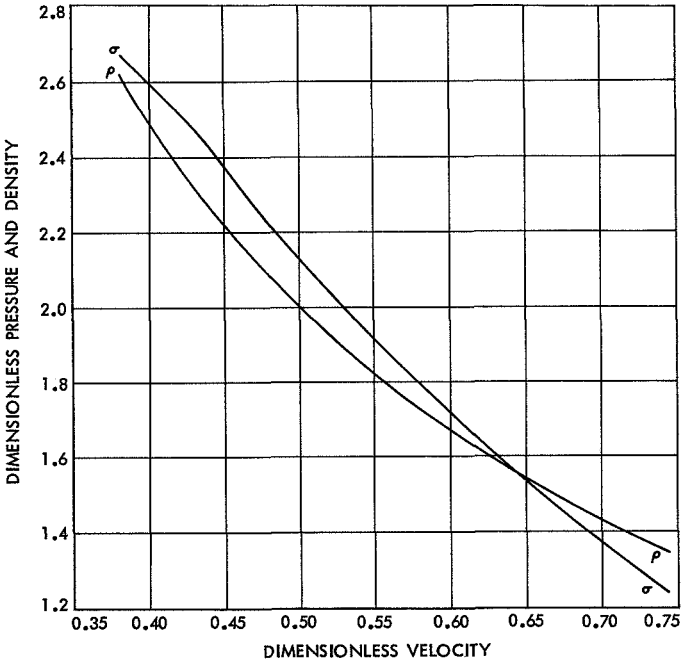

Fig. 24. Pressure and density vs velocity curves for $M = 1.5$, $N_R = 10$, and $N_V = 500$

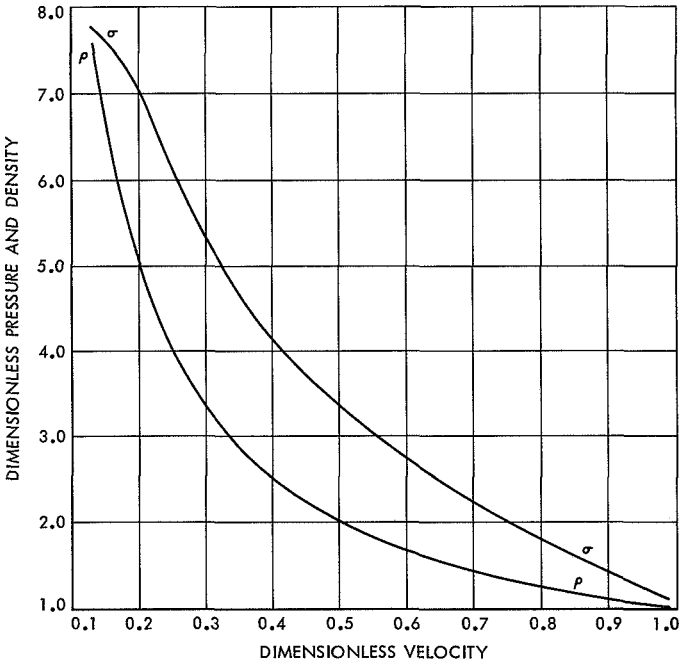

Fig. 25. Pressure and density vs velocity curves for $M = 10$, $N_R = 10$, and $N_V = 500$

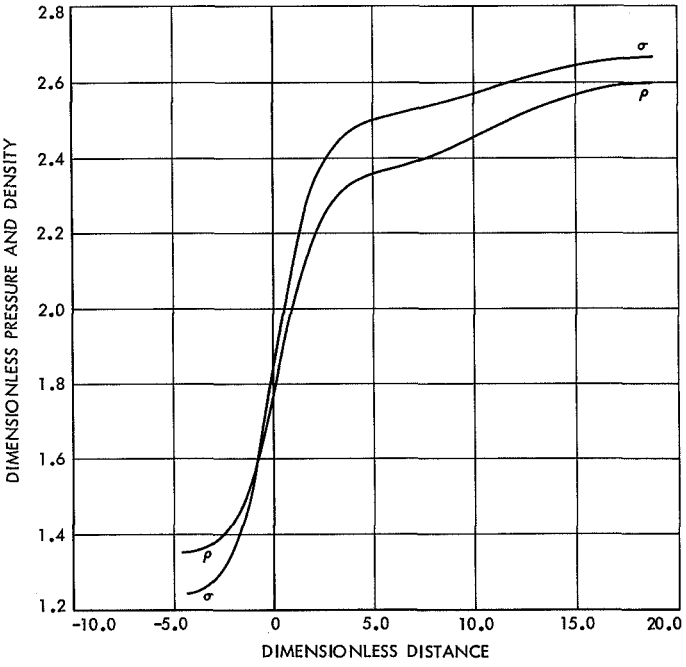

Fig. 26. Pressure and density vs distance curves for $M = 1.5$, $N_R = 10$, and $N_V = 500$

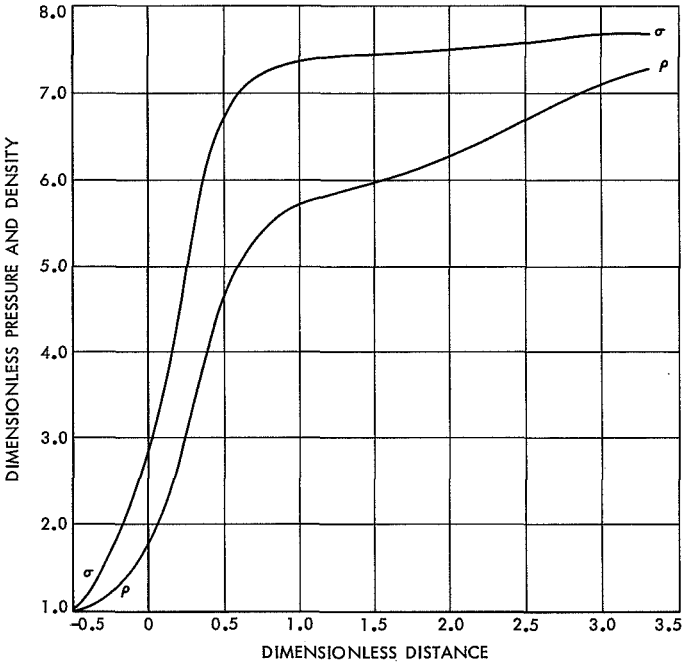

Fig. 27. Pressure and density vs distance curves for $M = 10$, $N_R = 10$, and $N_V = 500$

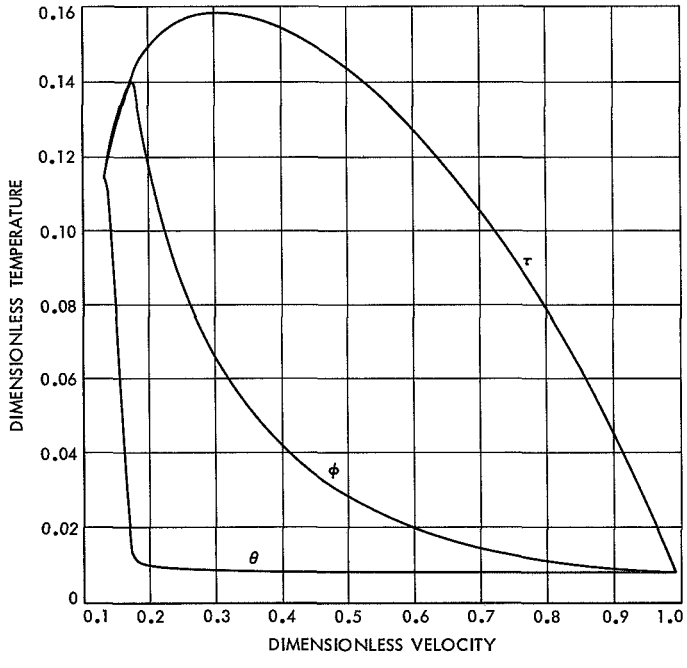

Fig. 28. Temperature vs velocity curves for $M = 10$, $N_R = 5$, and $N_V = 500$

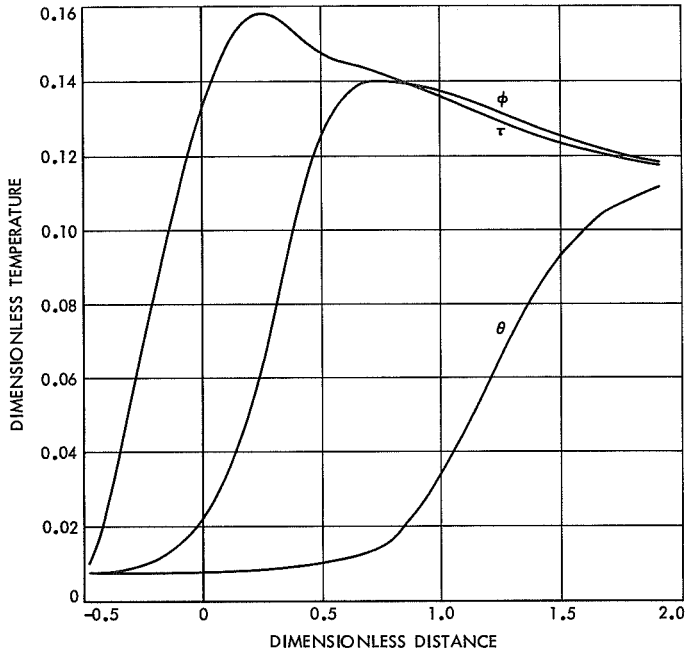

Fig. 29. Temperature vs distance curves for $M = 10$, $N_R = 5$, and $N_V = 500$

References

1. Talbot, L., and Scala, S. M., "Shock Wave Structure in a Relaxing Diatomic Gas," *Advances in Applied Mechanics: Supplement 1, Rarefied Gas Dynamics.* Academic Press, New York, 1961.

2. Scala, S. M., and Talbot, L., "Shock Wave Structure With Rotational and Vibrational Relaxation," *Advances in Applied Mechanics: Supplement 2, Rarefied Gas Dynamics.* Academic Press, New York, 1963.

3. Vincenti, W. G., and Kruger, C. H., *Introduction to Physical Gas Dynamics.* John Wiley & Sons, Inc., New York, 1965.

4. Hirschfelder, J. O., Curtiss, C. F., and Bird, R. B., *Molecular Theory of Gases and Liquids.* John Wiley & Sons, Inc., New York, 1954.

5. Eringen, A. Cemal, *Mechanics of Continua.* John Wiley & Sons, Inc., New York, 1967.

NASA — JPL — Coml., L.A., Calif.